Title

Nanosecond dynamics of influenza A/M2TM and an amantadine resistant mutant probed by time-dependent red shifts of a native tryptophan

Permalink

https://escholarship.org/uc/item/7gt5v7bd

Authors

Nanda, Vikas
Cristian, Lidia
Toptygin, Dmitri
et al.

Publication Date

2013-08-01

DOI

10.1016/j.chemphys.2012.12.018

Peer reviewed

Nanosecond Dynamics of InfluenzaA/M2TM and an Amantadine Resistant Mutant Probed by Time-Dependent Red Shifts of a Native Tryptophan

Vikas Nanda[1,2], **Lidia Cristian**[3], **Dmitri Toptygin**[4], **Ludwig Brand**[4], and **William F. DeGrado**[5]

[1]Center for Advanced Biotechnology and Medicine, Robert Wood Johnson Medical School – UMDNJ, Piscataway, New Jersey 08854

[2]Department of Biochemistry, Robert Wood Johnson Medical School – UMDNJ, Piscataway, New Jersey 08854

[3]Department of Biochemistry and Biophysics, School of Medicine, University of Pennsylvania, Philadelphia, Pennsylvania 1910-46059

[4]Department of Biology, Johns Hopkins University, Baltimore, Maryland 21218

[5]Department of Pharmaceutical Chemistry, University of California, San Francisco, CA 94158

Abstract

Proteins involved in functions such as electron transfer or ion transport must be capable of stabilizing transient charged species on time scales ranging from picoseconds to microseconds. We study the influenza A M2 proton channel, containing a tryptophan residue that serves as an essential part of the proton conduction pathway. We induce a transition dipole in tryptophan by photoexcitation, and then probe the dielectric stabilization of its excited state. The magnitude of the stabilization over this time regime was larger than that generally found for tryptophan in membrane or protein environments. M2 achieves a water-like stabilization over a 25 nanosecond time scale, slower than that of bulk water, but sufficiently rapid to contribute to stabilization of charge as protons diffuse through the channel. These measurements should stimulate future MD studies to clarify the role of sidechain versus non-bulk water in defining the process of relaxation.

Introduction

The M2 protein of the influenza A virus was first discovered as the protein target of the anti-influenza drug amantadine [1]. This modular protein serves multiple functions, which are localized in different domains of its short 97-residue sequence. M2 has a single transmembrane (TM) helix (Fig. 1) that serves as a tetramerization and proton-conducting domain. Conduction of protons into the virion acidifies the virus interior after endocytosis and initiates viral uncoating [2, 3]. Peptides spanning the TM domain reproduce most of the electrophysiological, pharmacological and biophysical features of the full-length protein, such as low-pH activated proton conductivity, amantadine sensitivity of the proton current, and tetramerization of the TM helix [4–6]. The small size and simple structure of this domain has made it an excellent candidate for biophysical studies [7–9].

Structures of M2's channel domain have been determined by solution NMR, Xray crystallography, and solids NMR [10–15]. These structures suggest a consistent mechanism for proton conduction. Protons enter the channel through a water-filled cavity that leads into the absolutely conserved residue, His37 (Fig. 1). A tetrad of His37 residues associate with four Trp41 sidechains (also absolutely conserved) in a stabilizing interaction that inhibits reverse flow of protons out of an acidified virus[16, 17]. The His37 tetrad is primed for conduction by binding two protons with high affinity[18, 19]; upon the protonation of a third His at the pH of the acidifying endosome, the channel opens. In the shuttle mechanism [20], addition of the third proton to the His37 tetrad from the extracellular side is followed by loss of a proton to the internal side, regenerating the +2 state. A high-resolution crystal structure [12] shows that the critical channel-lining residues – His37, Trp41, and Asp44 – lie in layers with well-ordered water clusters forming hydrogen-bonded bridges between each of these sidechains. A major question is how this basic structure flexes and adjusts as protons diffuse to and from His37, and as the charge on the His tetrad varies. MD simulations indicate that the crystallographic water positions are largely retained, although the water molecules are relatively mobile and exchange between preferred binding locations on the nanosecond time scale[12].

Infrared spectroscopic experiments have been used to examine the hydration and dynamics of Pore-lining residues in M2 on the femtosecond to low picosecond time scale, while NMR has been used to examine hydration and dynamics on the microsecond to nanosecond time scale. Hochstrasser and coworkers [21] used two-dimensional IR (2DIR) methods to determine the relaxation of the environment surrounding the carbonyl of G34, a group that lines the lumen of the channel near His37 (Fig. 1). At low pH, the probe is immersed in very mobile water with a correlation time of approximately 1.3 ps, but it senses structures having correlation times in excess of 10 ps at pH 8. At high pH, where the channel is poised to accept the arrival of a proton from the outside of the virus, any waters of hydration are immobilized on the 1 – 10 picosecond time scale. Solution NMR studies show that the Trp41 residue undergoes motions on the microsecond time scale that increase in rate with decreasing pH (and increasing His37 protonation) [14]. Solids NMR studies show that His37 sidechains undergo significant conformational motion at a rate at least an order of magnitude faster than the conduction rate, indicating that such motions may facilitate, and should not limit, proton release[19, 22, 23]. These studies also show that much of the channel is in contact with water molecules that exchange with bulk water (on the micro to millisecond time scale), and that the degree of hydration of the pore increases at low pH. These studies are also in broad agreement with crystallographic structures solved at multiple pH [12], although the crystallographic analysis shows structural changes that are larger than those inferred from solids NMR.

It would be interesting to study the time regime between picoseconds and microseconds probed in these 2DIR and the NMR studies. In pioneering work, Hochstrasser and coworkers measured dynamic stokes shifts of coumarin bound with the binding site of calmodulin to probe the picosecond to early nanosecond dynamics of this protein[24]. Similarly, tryptophan fluorescence is highly sensitive to dielectric relaxation of protein and solvent on the pico- to nanosecond timescale, making it an ideal probe for studying charge stabilization[25–27]. Photon absorption and excitation to the first singlet state results in a rapid redistribution of charge across the indole chromophore, followed by electrostatic relaxation of the protein and solvent environment. A typical red shift of the emission spectrum by 3500 cm^{-1} corresponds to ten kcal/mole energetic stabilization of the excited-state chromophore by the surrounding environment. Most of the relaxation is contributed by bulk solvent, which occurs within a few picoseconds at room temperature[28–30]. Such processes are too rapid to be detected in these measurements, although sub-picosecond measurements have been reported[31, 32]. However, additional relaxation of the protein can

extend to tens of nanoseconds. While it is common to characterize the complex emission intensity kinetics of tryptophans in proteins as time constants reflecting a sum of discrete exponential components, in this instance it is more appropriate to study the magnitudes and rates of relaxation as measured by the time dependent red-shift in the emission spectrum.

Here we examine the time-resolved emission spectra (TRES) of Trp41 in M2's TM domain in (M2TM peptide) in phospholipid bicelles. To probe the interaction between the His37 cluster and Trp41, we compared the fluorescence properties of M2TM with a variant in which His37 is mutated to Ala (H37A). The results are also compared with Mastoparan X (MX), an amphiphilic peptide with one tryptophan located in the membrane headgroup region of the bilayer [33]. The depth of the MX tryptophan in the membrane is roughly similar to that of W41 of M2TM, but it does not participate in protein-protein interactions. Finally, we examine an amantadine-resistant mutant of M2, L26F, which has reduced affinity for this drug [34, 35]. Mutations at this position near the exterior end of the bundle are known to cooperate with mutations on the opposite side of the channel[16], suggesting that this seemingly minor mutation might have effects that propagate throughout the length of the bundle. Indeed, MD simulations indicated that L26F increased the hydration of the pore and increased the dynamics of the helical bundle[35], making clear predictions that could be tested by fluorescence spectroscopy. We therefore also studied the L26F variant. All peptides were studied in DHPC/POPC bicelles, which mimic the natural bilayer environment better than micelles [36] and have the added benefit of minimizing experimental challenges associated with optical scattering by lipid bilayer vesicles. The results show that the environment surrounding the polar excited state of Trp41 in M2TM adjusts on the nanosecond time scale. His37 is critical to achieving the full stabilization. Furthermore, L26F behaves in a manner consistent with the results of MD simulation. Finally, binding of amantadine decreases the ability of the protein to stabilize the polar Trp excited state, and increases the heterogeneity of the underlying conformational dynamics.

Results

Steady state florescence spectra and acrylamide quenching

The steady state fluorescence spectra of M2TM at pH 4.5 and 8 shows that the Trp41 indole experiences a relatively polar environment, similar to bulk water. The only amino acid in M2TM that is effectively titratable in this pH range is His 37. In agreement with earlier studies[37], lowering the pH results in a slight red-shift of $_{bc}$ (barycenter of the spectrum) from 351 to 353 nm and a 1.5-fold reduction in emission intensity (Fig. 2, Table 1). In contrast, addition of amantadine to M2TM at pH 8.0 (amantadine binds most tightly at high pH) results in a two-fold enhancement in emission intensity and a blue-shift in $_{bc}$ to 346 nm. Previous work in our lab has shown that the fully amantadine resistant M2 mutant (V27S) does not show any fluorescence shift upon addition of amantadine, indicating that the observed change is due to specific changes in the channel environment and not nonspecific binding of Trp 41 to amantadine [5]. The mutant L26F also showed a shift in the emission maximum to shorter wavelengths upon addition of amantadine. By comparison, MX has a relatively blue-shifted spectrum, consistent with the exposure of its tryptophan to the lipid headgroup region of the bilayer.

The Stokes shift in a tryptophans's emission spectrum reflects its degree of solvent accessibility[27], as well as specific interactions with neighboring polar groups within the protein matrix that stabilize the excited state [38]. To help differentiate between these two effects, we measured the accessibility of Trp 41 to acrylamide, which is a collisional fluorescence quencher (Table 1). As seen previously using iodide quenching of the full-length protein, the accessibility of Trp41 in M2TM increases as the pH is lowered below 8 [39]. Acrylamide quenching gives a Stern-Volmer constant of 2.4 and 2.5 M^{-1} at pH 8 in the

presence and absence of amantadine. These values are significantly lower than the accessibility of a fully solvent exposed tryptophan (K_{sv} for N-acetyl-tryptophan-amide is approximately 17.5 M^{-1})[40], but higher than the accessibility of a tryptophan buried inside a protein (K_{sv} of tryptophans in the interfacial region of -hemolysin is around 0.58 M^{-1}) [41]. The intermediate accessibility at high pH is also consistent with the structure (Fig. 1), which shows the Trp near the external vestibule with one face partially accessible to solvent. At low pH the K_{sv} of M2TM increases to 3.3 M^{-1} indicative of an increase in hydration and accessibility of the channel seen in crystallographic structures and by solids NMR. Similar conclusions are reached comparing the second order rate constant for quenching, k_q. A similar value of K_{sv} is also seen for the mutant H37A. The accessibility of Trp41 to acrylamide in the WT at low pH is also similar to that seen in MX, which has a K_{sv} = 3.4 M^{-1}.

The accessibility of Trp41 is significantly greater in L26F than WT based on the values of K_{sv} and the corresponding k_Q. For example, the value of K_{sv} increases from 2.4 M^{-1} in WT to 4.5 M^{-1} in L26F. Moreover, K_{sv} does not change markedly at low pH and at high pH in the presence of amantadine. These data are consistent with the greater hydration and dynamic motion of L26F seen in previous MD simulations [42].

Dielectric relaxation of the Trp environment

While it is relatively common to characterize tryptophan emission kinetics as a sum of exponentials and their corresponding lifetimes, in this case measuring the time dependent red shift by following the evolution of the emission spectrum is more informative and provides insight into the dynamics of charge state stabilization and relaxation following an instantaneous change in local electrostatic interactions within the channel. Previous work has shown that the relaxation of bulk water is complete within a few picoseconds, which is beyond the resolution of our instrument [31]. Here, spectral relaxation is measured on the 50 picosecond to 25 nanosecond time scale, which is expected to report on conformational changes within the protein.

Time correlated single-photon counting data were collected across a series of wavelengths at five nanometer intervals over the emission spectrum of tryptophan (300–450 nm). Fitting of emission kinetics at single wavelengths required multiple exponentials (Fig. S1, Table S1). Global analysis of fluorescence data across multiple wavelengths resulted in time resolved emission spectra where spectral widths remained constant as the emission spectrum shifted to lower energies for all the peptides studied. The extent of relaxation for wild-type M2TM was reduced upon addition of amantadine (Fig. 3), suggesting that drug binding restricts dielectric relaxation within the proton channel. To explicitly characterize these effects, we subsequently fit the data to a model for the time-dependent red shift that quantifies the kinetics of the various relaxation processes.

The experimental method and data analysis for fitting time dependent red shifts is described in detail in previous work [43]. The peak emission frequency as a function of time is described as a sum of exponentials with relaxation times τ_i and amplitudes β_i (eq. 1).

$$\nu(t) = \nu_\infty + \sum_i \beta_i \cdot e^{-t/\tau_i} \quad \text{Eq. 1:}$$

M2TM shows a slow component in its dielectric relaxation, which accounts for much of the dielectric relaxation seen in this time regime. In all, four exponentials were required to describe the relaxation of M2TM, L26F, and H37A (Table 2). Multiple exponentials were required in similar measurements on other systems including indole in glycerol and protein GB1. The longest relaxation time for indole in glycerol at 20C was 4.4 ns [44], and 5.6 ns

for GB1 [43]. In contrast, M2TM shows a uniquely long time constant $_4$ which is on the order of twenty nanoseconds. Moreover, the amplitude of this component was greater than others, corresponding to approximately 70% of the positive amplitudes. Such long time constants are indicative of large scale motion coupled with dielectric relaxation and could be reflecting conformational changes within the channel upon excitation of W41. Supporting this explanation, the TRES data for MX require only three exponentials, and the longest time component was 7.2 nanoseconds.

Another unique feature of M2TM is the negative amplitude for the third exponential term. This feature indicates a nonlinear response that could be attributed to a damping force counteracting relaxation initiated by tryptophan excitation, or a delay in relaxation caused by interactions which are broken at some point after excitation to facilitate conformational change. In either case, the presence of this amplitude is indicative of a relatively rough energy landscape. It is interesting to note that the negative amplitude was greatest in the presence of amantadine, indicating that the binding of the drug increased the roughness of the landscape. On the other hand, the negative amplitude was near zero for H37A, indicating that this residue was needed for this response.

The value of $_0$ reflects the degree of stabilization of the excited state of the indole group following the initial relaxation of solvent in the sub- to low picosecond dead time of our instrument, while the value of reports on the degree of stabilization from motions in the 50 picosecond to 100 nanosecond time regime. After 25 nanoseconds fluorescence emission becomes too weak to reliably determine the emission spectrum, but the relaxation process does not cease by 25 nanoseconds. Therefore to determine , we extrapolated the relaxation curve slightly beyond the time range covered by the fluorescence data. For M2TM, the corresponding emission maxima ($_0$ and) shift from 341 to 363 nm in this time period (Table 3). A similar response is seen at pH 4.5 (Fig. 4). The final energy of the excited state of Trp41 in M2TM after 25 nanoseconds is similar to that of indole in water after one picosecond [44], indicating that M2 reaches a similar degree of stabilization by a much slower conformational process. By comparison, the Trp in MX remains in a less polar environment throughout this time period, and the net change in stabilization is smaller, as the values of $_0$ and of 333 and 347 nm (= 14 nm), respectively. Interestingly, the values of $_0$ and for H37A are both blue-shifted by 6 to 7 nm relative to WT, indicating that His37 plays an important role in stabilizing the excited state. However, the value of is the same for M2TM as H37A, suggesting that H37A retains some of the same motions. Amantadine has a small effect on $_0$ but a much larger effect on , causing a 12 nm shift of the fully relaxed emission spectrum to shorter wavelengths. Thus, the drug restricts the dielectric response, which is consistent with previous studies that showed that binding of drugs decrease the conformational mobility of M2TM [45, 46].

L26F behaves qualitatively similar to M2TM, but the values of $_0$ and are shifted by a few nm to shorter wavelengths. The addition of amantadine causes a smaller effect on and for L26F than on M2TM (Fig. 5). This is likely due to a slightly different mode of binding to M2TM. It is also possible, however, that the drug is not fully bound to this mutant, which has reduced affinity for amantadine.

Conclusions

As an excess proton diffuses through the M2 proton channel, it must be stabilized in a water-like environment that assures that it will neither experience any high-energy intermediates that would be difficult to overcome or deep energy wells from which it would be difficult to escape. Therefore, the channel must respond dielectrically to stabilize fluctuations in local charge on a time scale that is more rapid than the net rate of diffusion through the channel

(app. 0.1 to 1 microsecond). Here, we use the dielectric response to photoexcitation of Trp to probe the degree and kinetics of stabilization achieved in the M2 channel. We expect to observe two components to the relaxation: the first would involve reorientation of mobile waters in the vicinity of Trp41, which would occur on the femtosecond to low picosecond time scale and is not resolved here. The second slower portion of the relaxation is probed here, and found to occur in a multi-exponential process along a rough landscape. However, the final degree of stabilization is similar to that seen in water. Interestingly, this stabilization depends on the presence of the essential His37 residue. Furthermore, the degree of stabilization achieved in this process is dampened in the presence of amantadine, which is known to lock M2 into a more restricted ensemble of conformational states. The difference in for M2TM at pH 8 in the presence vs. absence of drug amounts to 915 cm^{-1}, which corresponds to 2.6 kcal/mol for WT; the corresponding values for L26F are 746 cm^{-1} and 2.1 kcal/mol, respectively. Therefore, amantadine binding to the wild-type channel reduces the protein's functional dynamics and its ability to stabilize charge by approximately ~ 2 to 3 kcals/mole.

Methods

Peptide Synthesis

All M2 peptides (M2TM, M2$_{19–62}$, M2TM L26F and M2TM H37A) were synthesized using FMOC chemistry on an Applied Biosystems 430A peptide synthesizer using methods described previously [4, 5]. The peptides were purified by reverse phase HPLC using a Vydac C-4 preparative column and a linear gradient of solvent B (6:3:1 2-propanol:acetonitrile:water; 0.1 % TFA) and solvent A (0.1 % TFA). The identities of the purified peptides were confirmed by MALDI-TOF (PerSeptive Biosystems, Framingham, MA) mass spectrometry and purity was assessed by analytical HPLC. Disulfide bonded homodimers were formed as described previously [47, 48]. Mastoparan X was purchased from Bachem Bioscience Inc., King of Prussia, PA, and was used without further purification.

Bicelle and Sample Preparation

The peptides were incorporated into bicelles composed of 1,2-dihexanoyl-sn-glycero-3-phosphocholine (DHPC) and 1-palmitoyl-2-oleoyl-sn-glycero-3-phosphocholine (POPC) (Avanti Polar Lipids, Alabaster, AL) with a total lipid content of 15% (w/v). Bicelle solutions were generated by first preparing a concentrated stock solution of DHPC in buffer (50 mM Tris, 50 mM NaCl, pH 8.0 and 4.5). An appropriate amount of this stock solution was then added to a weighted amount of POPC lipid followed by thorough mixing until the lipid was dissolved and the solution was clear. The bicelle mixture was then used to solubilize the peptides (in powder form), using repeated mixing, centrifugation and sonication. The final samples contained 40 M peptides, DHPC/POPC (5:1 mole ratio) and a peptide/POPC mole ratio of 1:100. Based on previous studies, under these conditions the M2 peptides are expected to adopt a fully tetrameric conformation [48]. Samples containing amantadine were prepared by adding an appropriate amount of amantadine from a stock solution in buffer to the samples to obtain a final concentration of 0.4 mM amantadine. In order to improve the stability of the bicelle systems at low pH, DHPC was substituted with 1,2-di-O-hexyl-sn-glycero-3-phosphocholine [36].

Time Resolved Fluorescence – Instrument and Sample Setup

Measurements were conducted on a single photon counting instrument constructed in the laboratory. The excitation pulse was generated by a picosecond dye laser, which was synchronously pumped by the frequency-doubled output of a mode-locked Nd:YAG laser (Spectra Physics 3000 series, Mountain View, CA). The visible light output of the dye laser

was frequency doubled to 291 nm in order to excite directly into tryptophan. The excitation pulse train was vertically polarized with 15 ps pulses separated by 245 ns intervals. Sample emission was collected at right angles by two microchannel plate photomultipliers and stored in 2048 channels (13.3 ps / channel). Emitted light passed through a polarizer set to the magic angle (55°) and a monochromator with 8 nm resolution. The impulse response function was determined by collecting a scattering signal using Ludox (Dupont, Wilmington, DE), a colloidal silica suspension. The excitation pulse from the scattering cell was 5 channels, or approximately 65 ps full width at half maximum. Neutral density filters were placed in the excitation beam path in order to prevent sample photobleaching. For each sample, thirty-one decay curves were acquired at emission wavelengths from 300 to 450 nm in 5 nm increments. Photons were counted for approximately five minutes per wavelength.

Analysis of Emission Kinetics

A model function representing multi-exponential decay kinetics was convolved with the impulse response and fit to the data using nonlinear least squares optimization.

$$F(\lambda_{em}, t) = \sum_i \alpha_i(\lambda_{em}) \cdot e^{-t/\tau_i} \quad \text{Eq. 2:}$$

Time constants (τ_i) were globally linked across all wavelengths and pre-exponential factors (α_i) were locally optimized using the program LGLOBAL [49]. A constant scattering correction term was introduced to all fits with τ = 0.013 ns.

Steady State Fluorescence

Steady state fluorescence spectra were collected on an SLM-48000 spectrofluorometer. Samples were excited at 291 nm with polarizers set to the magic angle, 55° and excitation slit width at 2 nm. Emission was collected from 295 to 460 nm in 1 nm increments with two scans averaged. Emission polarizers were set to vertical and slits were 4 nm. Fluctuations in lamp intensity were corrected using a rhodamine quantum counter and fluorescence intensities are reported as the ratio of protein emission to lamp intensity. In order to compare steady state fluorescence emission from different samples with variations in tryptophan concentration, spectra were normalized to absorbance at 295 nm. Absorbance at 295 nm was corrected for Rayleigh scattering by extrapolating absorbance from 320 to 400 nm using a constant over wavelength to the fourth power. Technical spectra were corrected for spectral variation in instrument sensitivity before use in any analysis presented. Barycenters of the steady state spectra (λ_{bc}) were calculated by an intensity-weighted average of *n* wavelengths.

$$\lambda_{bc} = \sum_n \lambda_n I_n \bigg/ \sum_n I_n \quad \text{Eq. 3:}$$

Acrylamide Quenching Titrations

To measure accessibility of Trp 41 to acrylamide, constructs of M2 were incorporated into bicelles as described. A 4.8 M stock solution of acrylamide was added to the bicelle suspension in 5 – 50 μL aliquots to cover a concentration range of 0 to 750 mM acrylamide. The sample was gently pipet-mixed and allowed to equilibrate for five minutes. The sample was excited at 295 nm and emission was monitored at 340 nm. Corrections were made for sample dilution due to addition of quencher. Emission intensity was plotted as the ratio of initial fluorescence over measured intensity. This was fit to a line, the slope of which was the Stern-Volmer quenching constant, K_{sv}.

K_{sv} values were used to calculate the bimolecular quenching constant, k_Q, using the average lifetime of the excited state, $\langle\tau\rangle$. $\langle\tau\rangle$ was computed by taking the sum of the area under the intensity weighted decay associated spectra (DAS) for each lifetime component (Table S1, Fig. S1):

$$\langle\tau\rangle = \sum_{i=1}^{5}\tau_i \cdot \left(\sum_{\lambda=305\ nm}^{450}\alpha_{i,\lambda}\cdot\tau_i\right)\Big/\sum_{i=1}^{5}\sum_{\lambda=305\ nm}^{450}\alpha_{i,\lambda}\cdot\tau_i \quad \text{Eq. 4:}$$

Where $_i$, is the pre-exponential factor for the lifetime component i at wavelength. k_Q was then determined by:

$$k_Q = K_{SV}/\langle\tau\rangle \quad \text{Eq. 5:}$$

Supplementary Material

Refer to Web version on PubMed Central for supplementary material.

References

1. Hay AJ, Wolstenholme AJ, Skehel JJ, Smith MH. EMBO J. 1985; 4:3021–3024. [PubMed: 4065098]

2. Pinto LH, Holsinger LJ, Lamb RA. Cell. 1992; 69:517–528. [PubMed: 1374685]

3. Pinto LH, Lamb RA. J. Biol. Chem. 2006; 281:8997–9000. [PubMed: 16407184]

4. Kochendoerfer GG, Salom D, Lear JD, Wilk-Orescan R, Kent SB, DeGrado WF. Biochemistry. 1999; 38:11905–11913. [PubMed: 10508393]

5. Salom D, Hill BR, Lear JD, DeGrado WF. Biochemistry. 2000; 39:14160–14170. [PubMed: 11087364]

6. Cady SD, Mishanina TV, Hong M. J. Mol. Biol. 2009; 385:1127–1141. [PubMed: 19061899]

7. Cady SD, Luo WB, Hu F, Hong M. Biochemistry. 2009; 48:7356–7364. [PubMed: 19601584]

8. Wang J, Qiu JX, Soto CS, DeGrado WF. Curr. Opin. Struct. Biol. 2011; 21:68–80. [PubMed: 21247754]

9. Grigoryan G, Moore DT, Degrado WF. Annu Rev Biochem. 2011; 80:211–237. [PubMed: 21548783]

10. Cady SD, Schmidt-Rohr K, Wang J, Soto CS, DeGrado WF, Hong M. Nature. 2010; 463:689–692. [PubMed: 20130653]

11. Cady SD, Wang J, Wu Y, DeGrado WF, Hong M. J. Am. Chem. Soc. 2011; 133:4274–4284. [PubMed: 21381693]

12. Acharya A, Carnevale V, Fiorin G, Levine BG, Polishchuk A, Balannick V, Samish I, Lamb RA, Pinto LH, DeGrado WF, Klein ML. Proc. Natl. Acad. Sci. U. S. A. 2010; 107:15075–15080. [PubMed: 20689043]

13. Stouffer AL, Acharya R, Salom D, Levine AS, Di Costanzo L, Soto CS, Tereshko V, Nanda V, Stayrook S, DeGrado WF. Nature. 2008; 451:596–599. [PubMed: 18235504]

14. Schnell JR, Chou JJ. Nature. 2008; 451:591–595. [PubMed: 18235503]

15. Sharma M, Yi M, Dong H, Qin H, Peterson E, Busath D, Zhou HX, Cross TA. Science. 2010; 330:509–512. [PubMed: 20966252]

16. Chizhmakov IV, Ogden DC, Geraghty FM, Hayhurst A, Skinner A, Betakova T, Hay AJ. J. Physiol. 2003; 546:427–438. [PubMed: 12527729]

17. Tang Y, Zaitseva F, Lamb RA, Pinto LH. J Biol Chem. 2002; 277:39880–39886. [PubMed: 12183461]

18. Hu J, Fu R, Nishimura K, Zhang L, Zhou HX, Busath DD, Vijayvergiya V, Cross TA. Proc. Natl. Acad. Sci. U.S.A. 2006; 103:6865–6870. [PubMed: 16632600]

19. Hu F, Schmidt-Rohr K, Hong M. J. Am. Chem. Soc. 2012; 134:3703–3713. [PubMed: 21974716]

20. Pinto LH, Dieckmann GR, Gandhi CS, Papworth CG, Braman J, Shaughnessy MA, Lear JD, Lamb RA, DeGrado WF. Proc Natl Acad Sci U S A. 1997; 94:11301–11306. [PubMed: 9326604]

21. Ghosh A, Qiu J, DeGrado WF, Hochstrasser RM. Proc. Natl. Acad. Sci. U. S. A. 2011; 108:6115–6120. [PubMed: 21444789]

22. Hu F, Luo W, Hong M. Science. 2010; 330:505–508. [PubMed: 20966251]

23. Hong M, Fritzsching KJ, Williams J. J. Am. Chem. Soc. 2012 Epub ahead of print.

24. Changenet-Barret P, Choma CT, Gooding EF, DeGrado WF, Hochstrasser RM. J. Phys. Chem. B. 2000; 104:9322–9329.

25. Beechem JM, Brand L. Annu Rev Biochem. 1985; 54:43–71. [PubMed: 3896124]

26. Chen Y, Barkley MD. Biochemistry. 1998; 37:9976–9982. [PubMed: 9665702]

27. Lakowicz, JR. Principles of Fluorescence Spectrosocopy. Second ed. New York: Kluwer; 1999.

28. Nilsson L, Halle B. Proc Natl Acad Sci U S A. 2005; 102:13867–13872. [PubMed: 16162674]

29. Peon J, Pal SK, Zewail AH. Proc Natl Acad Sci U S A. 2002; 99:10964–10969. [PubMed: 12177425]

30. Xu JH, Toptygin D, Graver KJ, Albertini RA, Savtchenko RS, Meadow ND, Roseman S, Callis PR, Brand L, Knutson JR. J Am Chem Soc. 2006; 128:1214–1221. [PubMed: 16433538]

31. Shen XH, Knutson JR. J Phys Chem B. 2001; 105:6260–6265.

32. Lu WY, Kim J, Qiu WH, Zhong DP. Chem Phys Lett. 2004; 388:120–126.

33. Whiles JA, Brasseur R, Glover KJ, Melacini G, Komives EA, Vold RR. Biophys J. 2001; 80:280–293. [PubMed: 11159401]

34. Abed Y, Goyette N, Boivin G. Antimicrob Agents Chemother. 2005; 49:556–559. [PubMed: 15673732]

35. Wang J, Ma C, Fiorin G, Carnevale V, Wang T, Hu F, Lamb RA, Pinto LH, Hong M, Klein ML, DeGrado WF. J Am Chem Soc. 2011; 133:12834–12841. [PubMed: 21744829]

36. Ottiger M, Bax A. J Biomol NMR. 1999; 13:187–191. [PubMed: 10070759]

37. Czabotar PE, Martin SR, Hay AJ. Virus Res. 2004; 99:57–61. [PubMed: 14687947]

38. Vivian JT, Callis PR. Biophys J. 2001; 80:2093–2109. [PubMed: 11325713]

39. Polishchuk AL, Lear JD, Ma C, Lamb RA, Pinto LH, Degrado WF. Biochemistry. 2010; 49:10061–10071. [PubMed: 20968306]

40. Eftink MR, Ghiron CA. Biochemistry. 1976; 15:672–680. [PubMed: 1252418]

41. Raja SM, Rawat SS, Chattopadhyay A, Lala AK. Biophys J. 1999; 76:1469–1479. [PubMed: 10049328]

42. Wang J, Ma C, Fiorin G, Carnevale V, Wang T, Hu F, Lamb RA, Pinto LH, Hong M, Klein ML, DeGrado WF. J. Am. Chem. Soc. 2011; 133:12834–12841. [PubMed: 21744829]

43. Toptygin D, Gronenborn AM, Brand L. J Phys Chem B. 2006; 110:26292–26302. [PubMed: 17181288]

44. Toptygin D, Brand L. Chem Phys Lett. 2000; 322:496–502.

45. Cady SD, Wang J, Wu Y, DeGrado WF, Hong M. J Am Chem Soc. 2011; 133:4274–4284. [PubMed: 21381693]

46. Li C, Qin H, Gao FP, Cross TA. Biochim. Biophys. Acta. 2007; 1768:3162–3170. [PubMed: 17936720]

47. Cristian L, Lear JD, DeGrado WF. Protein Sci. 2003; 12:1732–1740. [PubMed: 12876322]

48. Cristian L, Lear JD, DeGrado WF. Proc Natl Acad Sci U S A. 2003; 100:14772–14777. [PubMed: 14657351]

49. Hirshfield KM, Toptygin D, Grandhige G, Packard BZ, Brand L. Biophys Chem. 1998; 71:63–72. [PubMed: 9591360]

Highlights

- Examined nanosecond dynamics of essential tryptophan residue of M2 proton channel.

- Channel blocking drugs restrict the ability of M2 to stabilize charge.

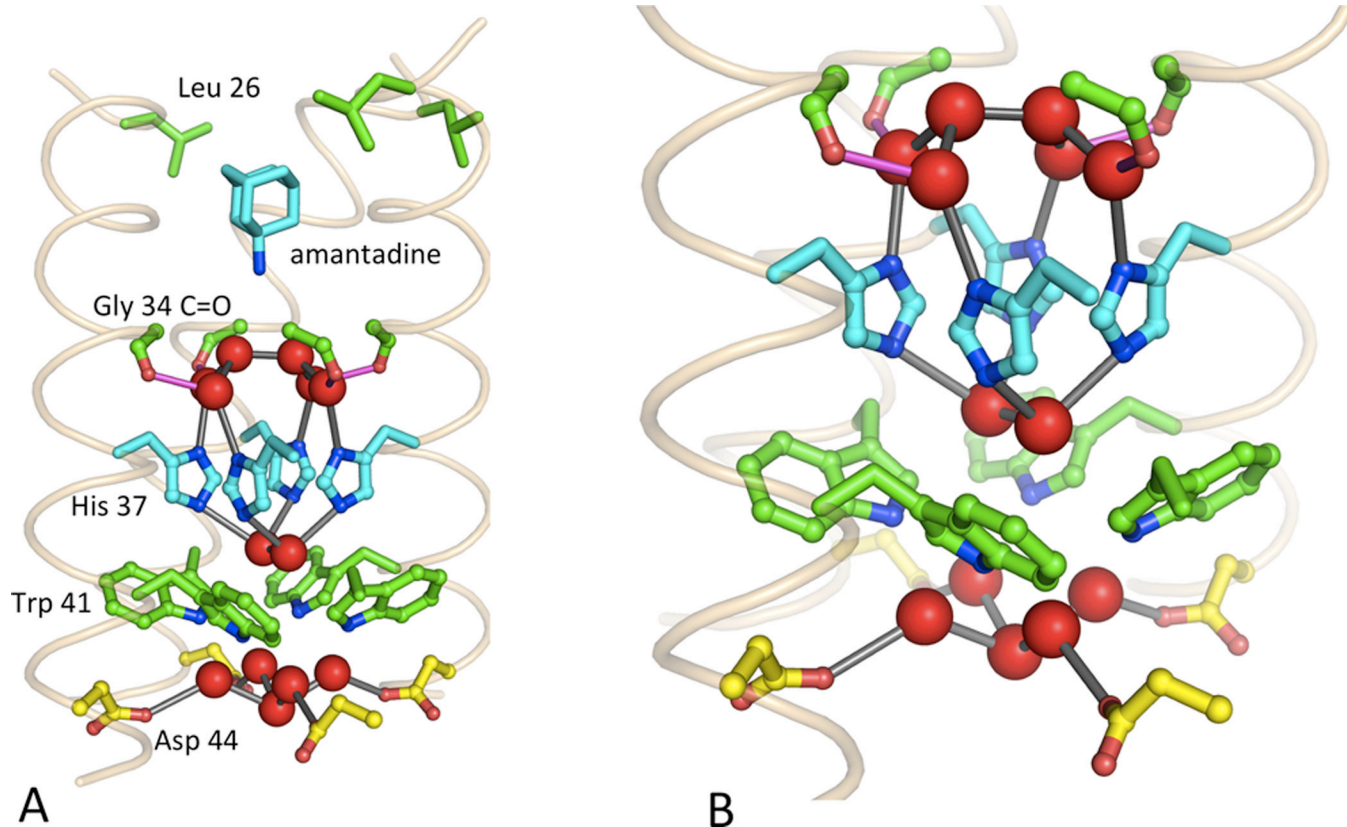- Dielectric relaxation of M2 consistent with molecular dynamics simulations studies.

Figure 1.
Structure of M2TM. The high-resolution structure solved at 1.65 Å [12]is shown in both panels. Panel A: The position of specific sidechains and the carbonyl of Gly34 are as indicated on the figure. Well ordered water molecules are in red balls, and the silver-grey tubes show the positions of hydrogen bonds between the waters or between waters and sidechains. The hydrogen bond to Gly34 is shown in magenta tubes. This structure was solved in the absence of amantadine, but the drug (light blue) is shown at the position seen in the very closely related solids NMR structure [10]. Panel B shows a larger view of the layers of His37, Trp41, and Asp44 sidechains and interspersed water clusters.
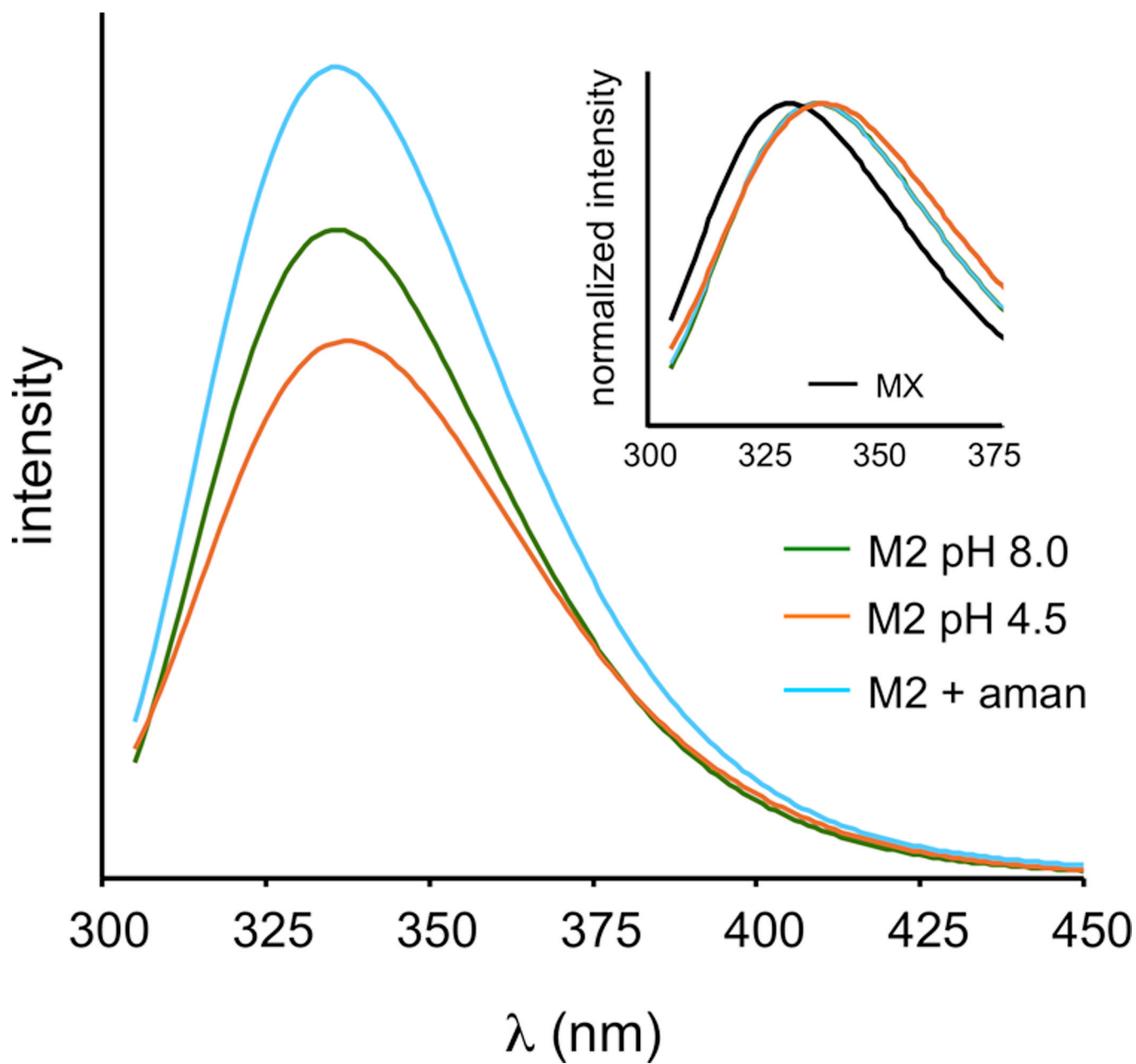
Figure 2.
Corrected, steady-state emission spectra of M2TM in bicelles at low and high pH and in the presence of excess amantadine. Spectra are peak-normalized on the right to highlight shifts in peak positions.
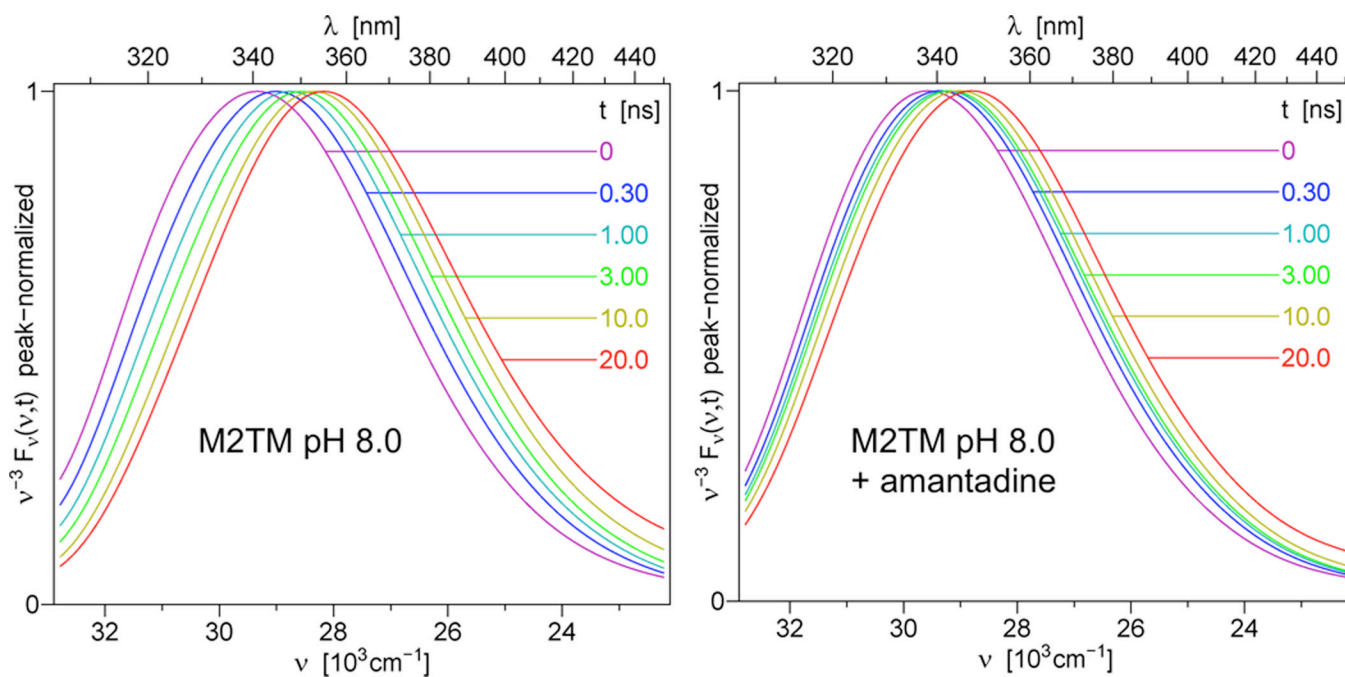
Figure 3.
Time resolved emission spectra (TRES) generated from the analysis of the multiple-wavelength W41 emission kinetics of M2TM with and without amantadine. Conservation of spectral shape over time is consistent with dielectric relaxation as a model for the shift in emission peak wavelength. Addition of amantadine retards the extent of dielectric relaxation occurring by twenty nanoseconds.
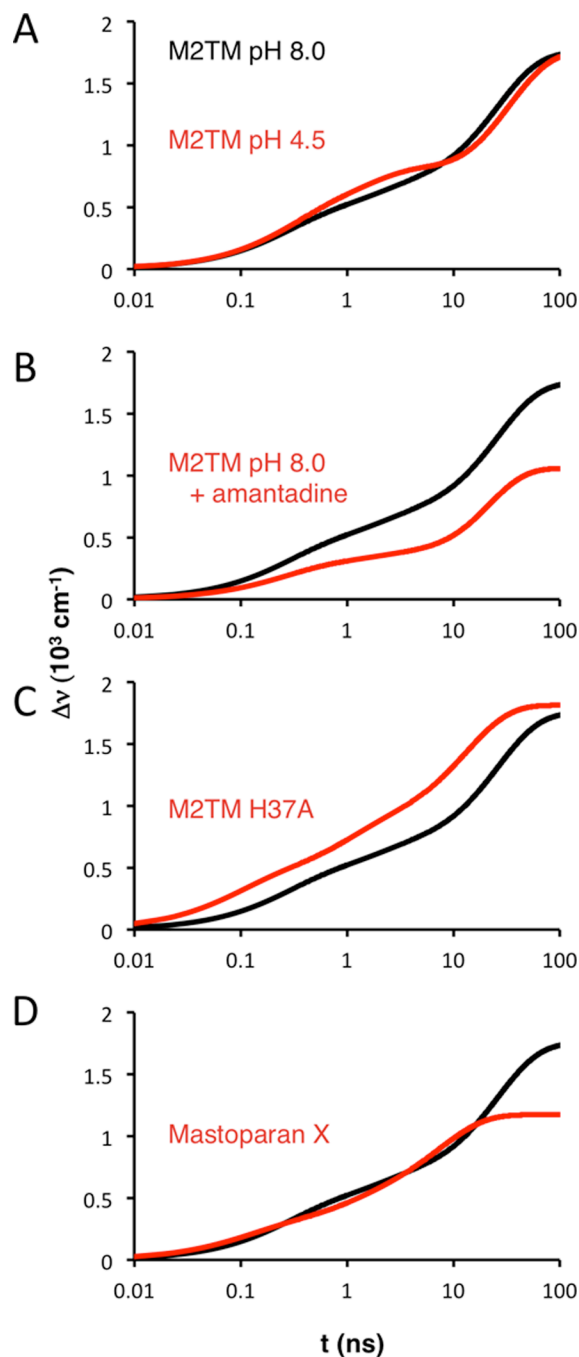
Figure 4.
Dielectric relaxation of wild-type M2TM under various environmental conditions. Relaxation is characterized as the shift in the emission spectrum barycenter relative to time zero. (A) M2TM is responsive to charge perturbations at both low and neutral pH. (B) Addition of amantadine retards the rate of relaxation and reduces the total extent of charge stabilization. (C) Mutating the adjacent histidine to alanine significantly perturbs kinetics of channel relaxation. (D) M2TM exhibits markedly different emission kinetics relative to the amphipathic membrane peptide mastoparan X. Black traces in all four panels correspond to M2TM at pH 8.0. Identity of red traces are indicated in each panel.
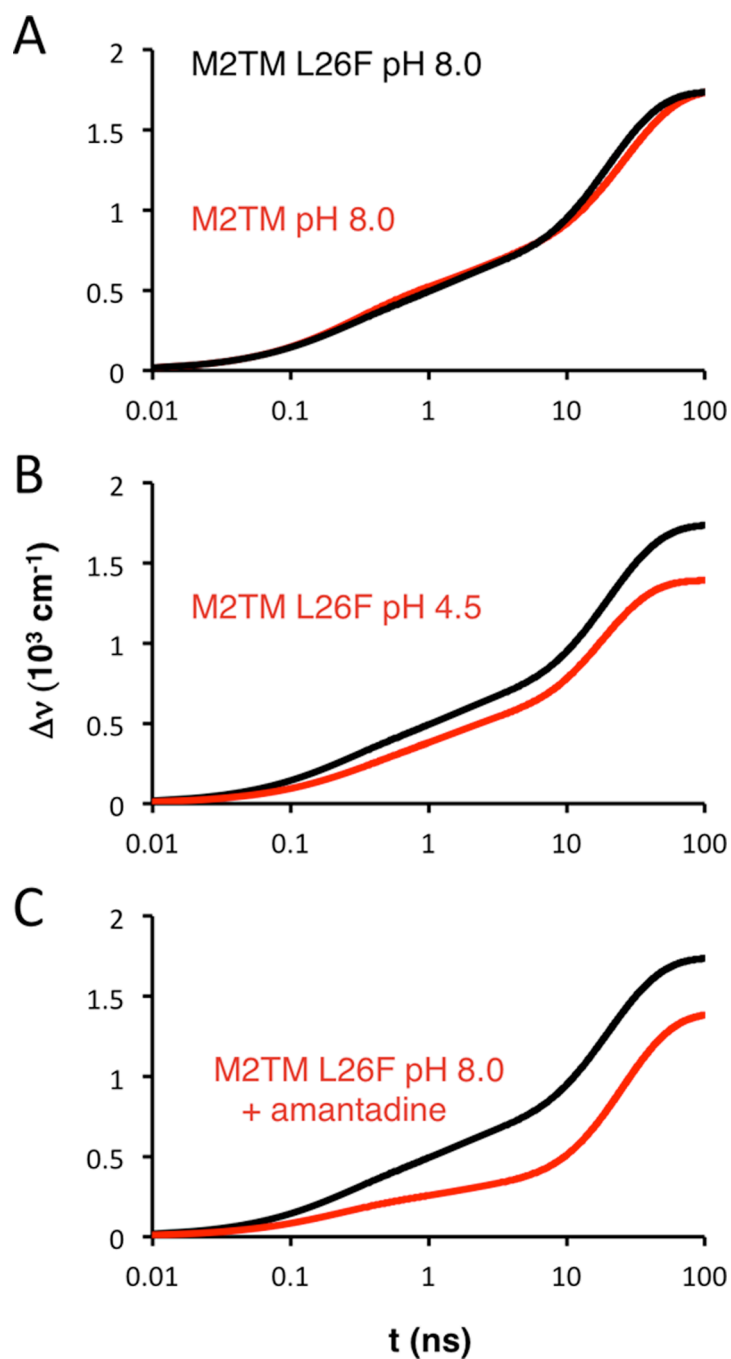
Figure 5.
Dielectric relaxation of the naturally occurring M2 mutant L26F at pH 8.0 compared with (A) wild-type M2TM, (B) L26F at acid pH and (C) L26F in the presence of amantadine. Black traces in all three panels correspond to M2TM L26F at pH 8.0. Identity of red traces are indicated in each panel.

Table 1

Steady state fluorescence and acrylamide quenching of peptides.

Peptide	Condition	b_c (nm)	K_{sv} (M^{-1})	< > (ns)	k_q (M^{-1}·ns^{-1})
WT	8.0	351.2	2.4	5.6	0.43
	4.5	353.1	3.3	5.1	0.65
	8.0 + AM	346.0	2.5	5.4	0.46
H37A		347.6	3.4	5.4	0.63
MX		342.7	3.3	3.8	0.87
L26F	8.0	349.9	4.5	5.1	0.88
	4.5	347.8	4.5	4.5	1.00
	8.0 + AM	345.2	4.2	5.1	0.82

Table 2

Multi-exponential fit of time dependent red shifts. Normalized amplitudes (c_i) given: $|\sum c_i|=1$.

Peptide	τ_1 (ns) c_1	2,2	3,3	4,4	ν_0 (cm^{-1})	(cm^{-1})	(cm^{-1})
M2TM pH 8.0	0.239 0.16	1.533 0.12	6.455 −0.12	23.006 0.59	29339	27586	1752
M2TM pH 4.5	0.253 0.14	1.547 0.18	6.332 −0.19	29.425 0.49	29437	27674	1763
M2TM pH 8.0 + AM	0.239 0.09	1.564 0.06	6.729 −0.29	14.952 0.55	29562	28501	1061
M2TM L26F pH 8.0	0.188 0.11	1.184 0.15	4.668 −0.16	17.283 0.59	29497	27756	1741
M2TM L26F pH 4.5	0.236 0.08	1.334 0.15	4.846 −0.22	14.196 0.55	29608	28214	1394
M2TM L26F pH 8.0 + AM	0.189 0.07	1.379 0.06	6.583 −0.24	20.299 0.63	29728	28332	1396
M2TM H37A	0.082 0.17	0.866 0.21	3.546 −0.07	12.0 0.55	29898	28083	1815
MX	0.097 0.20	0.734 0.15	7.223 0.65		30031	28857	1174

Table 3

Dielectric relaxation parameters.

Peptide	$_0$ (nm)	(nm)	(nm)	$E_{relaxation}$ kcals/mole	Relaxation Heterogeneity[a]
M2TM pH 8.0	340.8	362.5	21.7	5.0	0.14
M2TM pH 4.5	339.7	361.4	21.6	5.0	0.24
M2TM+AM	338.3	350.9	12.6	3.0	0.41
L26F	339.0	360.3	21.3	5.0	0.19
L26F+AM	336.4	353.0	16.6	4.0	0.31
L26F pH 4.5	337.7	354.4	16.7	4.0	0.28
H37A	334.5	356.1	21.6	5.2	0.08
MX	333.0	346.5	13.5	3.4	0.0

[a]Defined as the ratio of negative pre-exponential to the sum of positive pre-exponentials.